Tetrahedron 64 (2008) 11150–11158

Contents lists available at ScienceDirect

Tetrahedron

journal homepage: www.elsevier.com/locate/tet

# [1,2,3]Triazolo[1,5-*a*]pyridines. A theoretical (DFT) study of the ring–chain isomerization

Fernando Blanco [a,*], Ibon Alkorta [a], José Elguero [a], Víctor Cruz [b], Belén Abarca [c], Rafael Ballesteros [c]

[a] *Instituto de Química Médica, CSIC, Juan de la Cierva 3, E-28006 Madrid, Spain*
[b] *Instituto de Estructura de la Materia, CSIC, Serrano 113 bis, E-28006 Madrid, Spain*
[c] *Departamento de Química Orgánica, Facultad de Farmacia, Universidad de Valencia, Avda. Vicente Andrés Estellés s/n, E-46100 Burjassot, Valencia, Spain*

ARTICLE INFO

*Article history:*
Received 1 August 2008
Received in revised form
19 September 2008
Accepted 19 September 2008
Available online 30 September 2008

Dedicated to Gloria Ines Yranzo who untimely passed away in September 2008

*Keywords:*
Triazolopyridine
Isomerization
Substituent effects
Protonation
Deprotonation
Lithiation

ABSTRACT

The ring opening isomerization of [1,2,3]triazolo[1,5-*a*]pyridines to the corresponding 2-pyridyl derivatives has been studied by means of DFT calculations at the B3LYP/6-31+G(d,p) computational level. The effect of the substitution as well as those of protonation, deprotonation, and lithiation on different positions has been studied. The electronic characteristics of the optimized structures have been analyzed by means of the Atoms In Molecules (AIM), Electron Localization Function (ELF), Molecular Electrostatic Potential (MEP), and Natural Bond Orbital (NBO) methodologies.



## 1. Introduction

Ring–chain isomerism is an important property of many heterocyclic systems.[1,2] This process is often the first step of various chemical transformations and it is related to several fundamental properties of the heterocyclic systems, such as aromaticity and electronic structure as well as the nature of the heteroatoms.[3,4]

It is well known that the 1,2,3-triazole system presents ring–chain isomerism, as has been shown in several experimental and theoretical studies.[5–7] The mechanism of the decomposition of 1,2,3-triazoles and the thermodynamic stability of the cycle are governed in the first stage by the breaking of one bond of the cycle. Still, more related with the present investigation is the fact that in [1,2,3]triazolo[1,5-*a*]pyridines, a 1,2,3-triazole condensed heterocycle, the treatment with electrophiles, other than alkylating agents, like halogens, sulfuric and acetic acids, and selenium dioxide, afford products resulting from triazole ring opening with loss of molecular nitrogen. Two mechanisms, ionic and radical, have been proposed to explain this process,[8,9] starting from a ring–chain equilibrium in the 1,2,3-triazole ring (Scheme 1).

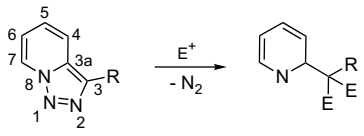


**Scheme 1.** Reaction of [1,2,3]triazolo[1,5-*a*]pyridines with electrophiles.

More recently, some of us carried out an experimental ($^1$H NMR) and theoretical (DFT) study of the ring–chain–ring isomerization of 3-(2-pyridyl)-[1,2,3]triazolo[1,5-*a*]pyrid-7-yl derivatives (**A**) into 6-(2-pyridyl) derivatives (**B**) (Scheme 2).[10] The experimental results as well as the calculations lead us to conclude that the **A**/**B** ratio depends on the electronic properties of the substituents.

* Corresponding author.
*E-mail address:* fblanco@iqm.csic.es (F. Blanco).

0040-4020/$ – see front matter © 2008 Elsevier Ltd. All rights reserved.
doi:10.1016/j.tet.2008.09.064

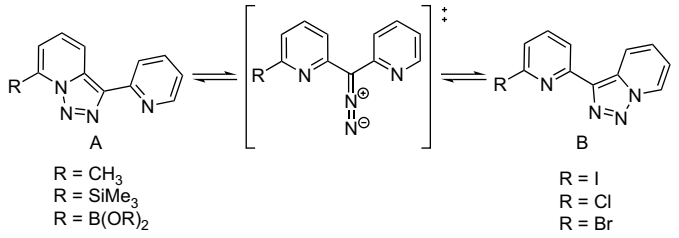


**Scheme 2.** Ring–chain–ring isomerization of 3-(2-pyridyl)-[1,2,3]triazolo[1,5-*a*]pyrid-7-yl. The substituents that favor each structure are indicated.

In the present work we decided to undertake the general study of the energetic profile and geometrical changes in the ring–chain isomerization process of [1,2,3]triazolo[1,5-*a*]pyridines, and the effects induced by the substitution, protonation, and deprotonation over the equilibrium. In addition, the electronic characteristics of the structures obtained have been analyzed out by means of the Atoms In Molecules (AIM), Electron Localization Function (ELF), Molecular Electrostatic Potential (MEP), and Natural Bond Orbital (NBO) methodologies. Finally, it was decided to include a specific study of the lithiation reaction, the most widely used method of functionalization of triazolopyridines, and the possible influence of the open forms on this process.

## 2. Computational methods

All molecular geometries have been fully optimized using the hybrid HF/DFT B3LYP method,[11,12] using the 6-31+G(d,p) basis set[13] combined with the ultrafine grid option and the Berny optimization algorithm as per the Gaussian-03 package.[14] Beyond this, default parameters were used. Frequency calculations have been carried out at the same computational level to confirm that all relevant structures correspond to energetic minima or real transition states.

The electron density topology and atomic properties have been evaluated within the AIM methodology[15] with the AIMPAC[16] and Morphy98[17] programs. A Natural Bond Orbital analysis,[18] using the NBO program,[19] has been used to study electronic parameters. The electrostatic potential generated by the molecule upon its surroundings has been calculated using the facilities within the Gaussian-03 package and the minimum in this potential has also been localized and evaluated. Such minima in the molecular electrostatic potential (MEP) have been widely used to analyze a priori the reactivity and complex formation of molecules,[20–22] and a similar analysis is carried out here.

The topological analysis of the ELF[23,24] has been extensively used for the analysis of chemical bonding as well for investigating chemical reactivity. ELF is a function that becomes large in regions of space where electron pairs are localized, either as bonding or lone pairs. The function is conveniently scaled between 0 and 1, thereby mapping from the very low (0) to very high (1) electron localization regimes. ELF isosurfaces thus provide clear pictures of the regions of electron localization in molecules. The attraction basins of ELF have been successfully related to key bonding concepts, such as core, valence, and lone-pair regions, while their populations and synaptic orders have been related to bond order. A convenient value of ELF=0.7 has been adopted for all the systems investigated in this study. Relevant bonding features of triazolopyridine are well discriminated at this ELF value, and the use of a common value for the isosurfaces ensures that a direct comparison among these molecules can be made.

## 3. Results and discussion

### 3.1. Neutral systems

The ring expansion of triazole moiety in [1,2,3]triazolo[1,5-*a*]pyridines (Scheme 3) is a moderately endothermic process. The reaction path starts by an increase of the distance of the N1N8 bond through an initial transition state **TS1** to a 2-diazomethylpyridine minimum **OPN1**. The second step is a rotational process through an 'orthogonal' transition state **TS2** to a second open minimum **OPN2**, with the diazo system oriented in the opposite side. **OPN1** and **OPN2** are 31 and 34 kJ mol$^{-1}$, respectively, less stable than the initial form **CLS**. The relative energy of the opening **TS1** and rotational **TS2** transition state structures are 82 and 71 kJ mol$^{-1}$, respectively. The larger dipole of **CLS** indicates that, as a first approximation, this configuration should be favored in polar environment. For comparative purposes the MP2/6-311++G(d,p) profile of this reaction (Table 1) has been calculated showing to be similar to the B3LYP one. The larger barrier obtained with the MP2 computational level is in agreement with previous reports that compared B3LYP and MP2 TS barriers.[25,26]

The initial structure **CLS**, opening transition state **TS1** as well as the **OPN1** and **OPN2** minima have planar geometries ($C_s$ symmetries). **TS2** ($C_1$ symmetry) has the diazo system located perpendicular to the pyridine plane. In the case of **CLS**, the similar bond distances in the triazole ring indicate its aromatic character. Table 2 shows the geometries of the different isomers, three substituted [1,2,3]triazolo[1,5-*a*]pyridines determined by X-ray crystallography being included.

**OPN1** and **OPN2** have clearly localized single (C3C3a) and double bonds (N1N2, N2C3, and C3aN8). The bond and angle values of the diazo group are similar to those experimentally described for diazomethane (CNN 180.0°, HCN 116.5°). The NN bond is longer than the N≡N bond in $N_2$ (1.097 Å)[27] but much shorter than an N=N bond in azoalkanes (1.493 Å).[28] The CN bond distance correspond to C($sp^2$)=N($sp^3$) bonds (1.279–1.329 Å).

Figure 1 shows the ELF representation for the **CLS**, **TS1**, and **OPN1** isomers. The electronic distribution in **CLS** is clearly aromatic with two lone pairs over N1 and N2. **TS1** shows an electronic reorganization, decreasing the density of charge in N2 in favor of the pyridinic nitrogen. **OPN1** is a diazo substituted pyridinic ring with a well-defined lone pair on the pyridinic nitrogen.

The electronic configuration of diazo compounds involves a positive charge on the central nitrogen and a negative charge

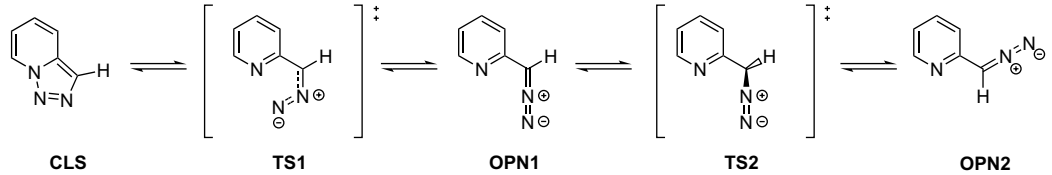


**Scheme 3.** Ring–chain isomerism of [1,2,3]triazolo[1,5-*a*]pyridines.

**Table 1**
Total (hartree), relative energies, and dipole moment of the ring–chain interconversion of [1,2,3]triazolo[1,5-*a*]pyridine calculated at B3LYP/6-31+G** and MP2/6-311++G** level

| Form | Sym | B3LYP/6-31+G** | $\Delta E$ (kJ mol$^{-1}$) | $\mu$ (debye) | MP2/6-311++G** | $\Delta E$ (kJ mol$^{-1}$) | $\mu$ (debye) |
|---|---|---|---|---|---|---|---|
| **CLS** | $C_s$ | −395.877959 | 0.0 | 5.09 | −394.841800 | 0.0 | 5.33 |
| **TS1** | $C_s$ | −395.846879 | 81.6 | 3.27 | −394.797522 | 116.3 | 2.75 |
| **OPN1** | $C_s$ | −395.866180 | 30.9 | 3.16 | −394.826197 | 41.0 | 2.88 |
| **TS2** | $C_1$ | −395.850796 | 71.3 | 3.51 | −395.812777 | 76.2 | 2.86 |
| **OPN2** | $C_s$ | −395.865006 | 34.0 | 1.50 | −395.823799 | 47.3 | 1.53 |

**Table 2**
Geometry (Å, °) of [1,2,3]triazolo[1,5-*a*]pyridine isomers calculated at B3LYP/6-31+G** level

| Form | N8N1 | N1N2 | N2C3 | C3C3a | C3aN8 | C3aC4 | C4C5 | C5C6 | C6C7 | C7 N8 |
|---|---|---|---|---|---|---|---|---|---|---|
| **CLS** | 1.361 | 1.314 | 1.351 | 1.396 | 1.389 | 1.419 | 1.374 | 1.430 | 1.366 | 1.371 |
| | *1.373*[a] | *1.328*[a] | *1.341*[a] | *1.392*[a] | *1.380*[a] | *1.405*[a] | *1.356*[a] | *1.406*[a] | *1.371*[a] | *1.408*[a] |
| | *1.351*[b] | *1.340*[b] | *1.360*[b] | *1.396*[b] | *1.369*[b] | *1.405*[b] | *1.350*[b] | *1.413*[b] | *1.330*[b] | *1.381*[b] |
| | *1.369*[c] | *1.307*[c] | *1.358*[c] | *1.395*[c] | *1.367*[c] | *1.396*[c] | *1.351*[c] | *1.408*[c] | *1.331*[c] | *1.367*[c] |
| **TS1** | 2.083 | 1.183 | 1.335 | 1.435 | 1.348 | 1.417 | 1.383 | 1.410 | 1.388 | 1.339 |
| **OPN1** | — | 1.141 | 1.306 | 1.454 | 1.348 | 1.411 | 1.390 | 1.399 | 1.396 | 1.337 |
| **TS2** | — | 1.147 | 1.297 | 1.495 | 1.345 | 1.403 | 1.396 | 1.394 | 1.398 | 1.339 |
| **OPN2** | — | 1.145 | 1.302 | 1.456 | 1.349 | 1.411 | 1.390 | 1.398 | 1.396 | 1.337 |

| Form | N8N1N2 | N1N2C3 | N2C3C3a | C3C3aN8 | C3aN8N1 | N8C3aC4 | C3aC4C5 | C4C5C6 | C5C6C7 | C6C7N8 | C7N8C3a |
|---|---|---|---|---|---|---|---|---|---|---|---|
| **CLS** | 106.5 | 110.7 | 108.9 | 102.9 | 111.1 | 118.2 | 119.0 | 120.5 | 120.4 | 118.4 | 123.5 |
| | *105.6*[a] | *111.8*[a] | *107.6*[a] | *104.8*[a] | *110.1*[a] | *120.6*[a] | *118.5*[a] | *119.9*[a] | *123.7*[a] | *115.3*[a] | *122.1*[a] |
| | *106.3*[b] | *110.4*[b] | *107.3*[b] | *104.9*[b] | *111.1*[b] | *117.7*[b] | *119.1*[b] | *121.1*[b] | *120.4*[b] | *118.2*[b] | *123.4*[b] |
| | *106.0*[c] | *110.1*[c] | *108.6*[c] | *103.0*[c] | *111.7*[c] | *117.8*[c] | *119.3*[c] | *120.3*[c] | *121.2*[c] | *117.7*[c] | *123.7*[c] |
| **TS1** | 90.8 | 130.1 | 109.1 | 113.5 | 96.5 | 120.1 | 118.6 | 120.2 | 118.1 | 121.6 | 121.5 |
| **OPN1** | — | 179.3 | 120.5 | 117.8 | 77.7 | 122.3 | 118.7 | 119.2 | 117.8 | 124.0 | 117.9 |
| **TS2** | — | 178.9 | 120.0 | 117.3 | 52.8 | 122.4 | 119.1 | 118.6 | 118.3 | 123.6 | 118.0 |
| **OPN2** | — | 179.1 | 122.0 | 114.4 | 20.4 | 122.3 | 118.7 | 119.3 | 117.8 | 124.0 | 117.9 |

[a] CSD refcode ARADEC.
[b] CSD refcode HETVAD.
[c] CSD refcode ZIBYIS.

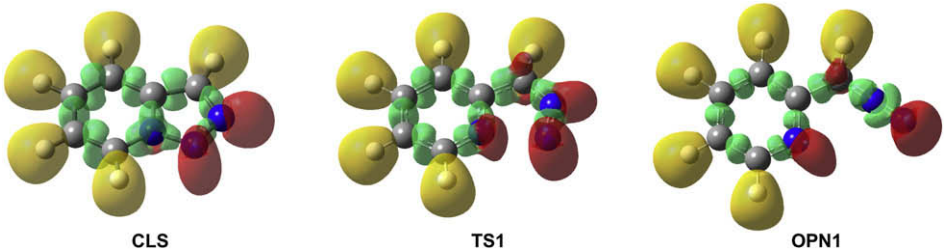


**Figure 1.** Representation of ELF for [1,2,3]triazolo[1,5-*a*]pyridines isomers (ELF 0.70). The nature of the attractor defining the domain is given by the color code. Yellow: valence protonated disynaptic; green: valence disynaptic; red: valence (lone pair).

distributed between the terminal nitrogen and the carbon with several resonance structures (Scheme 4).

The analysis of the ELF for **OPN1** shows two defined double bonds between CN and NN, and the lone pair localized over the terminal nitrogen, suggesting in this case a major contribution of the first resonance structure **a**. This result agrees with the bond distances previously discussed.

We have evaluated the charges of the systems using the NBO methodology (Table 3). As expected, the main variations occur in the triazole region. The evolution of the charge distribution of the nitrogen atoms is in good agreement with the ELF results, increasing the negative charge in N8 and decreasing in N2 in **OPN1** with respect to those in **CLS**. It is significant to note that the increment of negative charge in C3 from **CLS** to **OPN1** could be due to

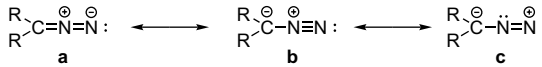


**Scheme 4.** Resonance structures of diazo system.

**Table 3**
Values of the NBO natural charges for the three structures considered

| Atom | CLS | TS1 | OPN1 |
|---|---|---|---|
| N8 | −0.19 | −0.42 | −0.48 |
| N1 | −0.11 | 0.03 | 0.02 |
| N2 | −0.24 | −0.07 | 0.06 |
| C3 | −0.12 | −0.23 | −0.25 |
| C3a | 0.10 | 0.16 | 0.16 |
| C4 | −0.23 | −0.26 | −0.28 |
| C5 | −0.24 | −0.20 | −0.20 |
| C6 | −0.29 | −0.31 | −0.31 |
| C7 | 0.01 | 0.04 | 0.02 |

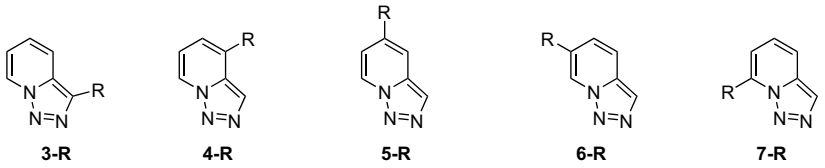


Series 1. R = F, $SiH_3$ (all the strutures)

Series 2. R = F, Cl, Br, H, $CH_3$, $SiH_3$ (only for 3-R and 7-R)

**Scheme 5.** Series of substituted [1,2,3]triazolo[1,5-*a*]pyridines considered.

**Table 4**
Relatives energies (kJ mol$^{-1}$) of the structures studied in Series 1 calculated at B3LYP/6-31+G** level

| Form | 3-F | 4-F | 5-F | 6-F | 7-F |
|---|---|---|---|---|---|
| **CLS** | 0.0 | 0.0 | 0.0 | 0.0 | 0.0 |
| **TS1** | 102.8 | 77.2 | 74.4 | 78.8 | 53.0 |
| **OPN1** | 61.6 | 23.5 | 20.9 | 23.4 | −14.4 |
| **TS2** | 103.4 | 67.0 | 63.5 | 61.0 | 28.3 |
| **OPN2** | 75.7 | 31.6 | 24.4 | 26.3 | −11.1 |
| Form | 3-$SiH_3$ | 4-$SiH_3$ | 5-$SiH_3$ | 6-$SiH_3$ | 7-$SiH_3$ |
| **CLS** | 0.0 | 0.0 | 0.0 | 0.0 | 0.0 |
| **TS1** | 76.6 | 83.7 | 83.3 | 80.1 | 91.4 |
| **OPN1** | 24.4 | 35.8 | 33.3 | 30.6 | 44.1 |
| **TS2** | 54.8 | 73.6 | 73.6 | 73.8 | 84.7 |
| **OPN2** | 16.6 | 52.7 | 36.7 | 34.0 | 47.1 |

the contribution of the two resonance species **b** and **c** of the diazo system (Scheme 4) where the negative charge is located on the carbon atom.

### 3.2. Substitution effects

We have calculated two series of *C*-substituted [1,2,3]triazolo[1,5-*a*]pyridines to check the substitution effect on the isomeric equilibrium. In an initial approach we analyzed the substitution in all the carbons that can be functionalized (C3, C4, C5, C6, and C7) with two groups with opposite electronegativity (R=F and R=$SiH_3$) and compared the results with those of the initial equilibrium (R=H) (Scheme 5).

Table 4 shows the relative energies of the functionalized isomers at the different positions. The substitution of the position (C4, C5, and C6) does not produce very significant differences with respect to the values in the parent equilibrium (R=H, Table 1). The larger variations occur in the 3- and 7-derivatives. Thus, it was decided to focus our research on these two specific positions.

The energetic effects of the two groups are very different. Figure 2 shows that the variation of the relative energies is more marked in the case of fluorine substitution. In the **3-F** series we observe a stabilization of the **CLS** form with respect to **OPN1** and **OPN2** with an increment of the relative energies of the TS structures. In contrast, the fluorine group in C7 (**7-F**) produces a considerable decrease of the transition state energies, resulting in the open isomers being more stable. The effect of the electron donating silyl group in the same substituted positions is lower but clearly opposite. It stabilized the open forms in C3 (**3-$SiH_3$**) and induces destabilization in the cases of the C7 substitution (**7-$SiH_3$**).

To complete the study, a second series of derivatives with intermediate electronegativity groups (Cl, Br, and $CH_3$) has been calculated, in addition to that previously studied (H, F, $SiH_3$). As seen in Table 5 there is a trend in function of the electronic character of the substituent. The closed isomer **CLS** is gradually stabilized versus the open ones (**OPN1** and **OPN2**) in order of the increasing electron withdrawing character of the groups in the position C3. Meanwhile the same groups localized in the position C7 produce a progressive destabilization (Fig. 4).

The regularities observed in Figure 2 mean that all columns of Table 5 are correlated ($0.880<R<0.999$) and also correlated with Hammett $\sigma_m$ albeit only moderately ($0.688<R<0.919$). We have represent (Fig. 3) the relationship between **TS1-7** and **TS2-7**.

We can deduce that the substitution modify the thermodynamic properties of the equilibrium, principally in the first opening step. Along with these lines and related with the Hammond postulate,[29] which predicts that the structure of the transition states resembles much more the structure of the energetically closest minima (starting products in exothermic reactions and final products in endothermic reactions), we have evaluated an arbitrary geometrical parameter (N8N1 distance) of **TS1** transition states versus the relative energy of **TS1** and **OPN1** isomers. In each case we found an interesting correlation (Fig. 5). The lowest value of the distance N1N8 (structurally closest to **CLS** geometry)

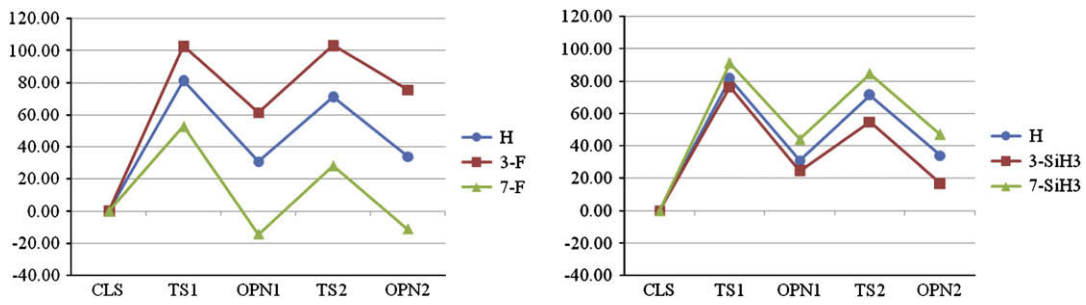


**Figure 2.** Substitution effect in the relative energies of Series 1 at C3 and C7 positions (kJ mol$^{-1}$).

**Table 5**
Relatives energies (kJ mol$^{-1}$) of the structures studied in Series 2 calculated at B3LYP/6-31+G** level

| Form | 3-$SiH_3$ | 3-$CH_3$ | 3-Br | 3-Cl | 3-F |
|---|---|---|---|---|---|
| **CLS** | 0.0 | 0.0 | 0.0 | 0.0 | 0.0 |
| **TS1** | 76.6 | 89.0 | 90.6 | 93.8 | 102.8 |
| **OPN1** | 24.4 | 42.9 | 45.6 | 51.4 | 61.6 |
| **TS2** | 54.8 | 81.3 | 84.1 | 86.7 | 103.4 |
| **OPN2** | 16.6 | 42.6 | 55.0 | 61.9 | 75.7 |
| Form | 7-$SiH_3$ | 7-$CH_3$ | 7-Br | 7-Cl | 7-F |
| **CLS** | 0.0 | 0.0 | 0.0 | 0.0 | 0.0 |
| **TS1** | 91.4 | 84.0 | 64.3 | 62.7 | 53.0 |
| **OPN1** | 44.1 | 35.6 | 4.9 | 1.4 | −14.4 |
| **TS2** | 84.7 | 75.9 | 47.9 | 43.7 | 28.3 |
| **OPN2** | 47.1 | 39.0 | 7.7 | 4.6 | −11.1 |

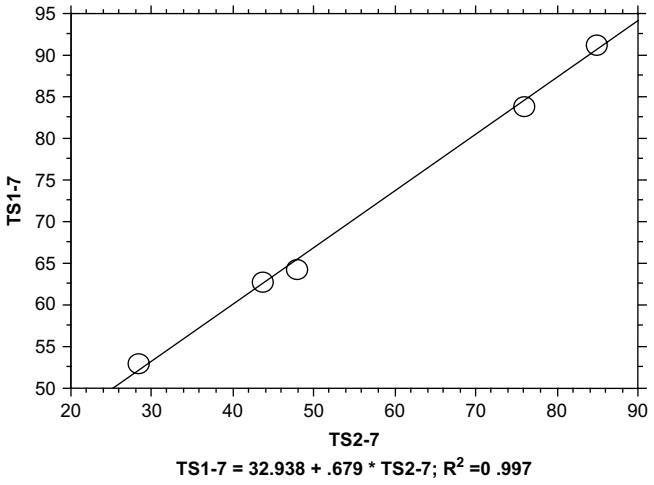


**Figure 3.** Relationship between **TS1-7** and **TS2-7**.

corresponds to the **7-F** derivative, which presents the most exothermic profile of reaction. The highest one (structurally closest to the **OPN1**) belongs to the **3-F** derivative, the most endothermic of the studied cases.

On the other hand, the stability of the **TS1** transition states can be evaluated through their molecular hardness ($\eta$) values. Molecular hardness is a concept introduced by Parr and Pearson,[30] which represents the chemical stability of a system. Hardness is defined as the second derivative of the total energy respect to the number of electrons, *N*, at constant chemical potential.

$$\eta = \frac{1}{2}\left(\frac{\partial^2 E}{\partial^2 N}\right)_{\upsilon(\mathbf{r})}$$

In numerical applications, $\eta$ is calculated through the following approximate equation based upon the finite difference

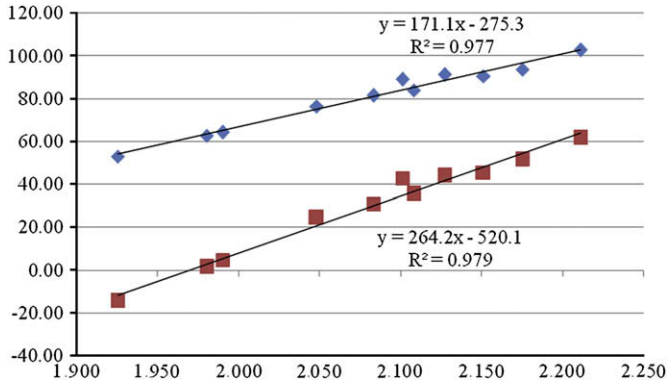


**Figure 5.** N2N8 distance (Å) in **TS1** versus $E_{rel}$ (kJ mol$^{-1}$) of **TS1** (blue) and **OPN1** (red).

approximation and Koopman's theorem,[31] where $\varepsilon_L$ and $\varepsilon_H$ are, respectively, the LUMO and HOMO energies.

$$\eta \simeq \frac{1}{2}(\varepsilon_L - \varepsilon_H)$$

We have found that the stability of the different **TS1** transition states measured through their $\eta$ values correlates well with the relative energies in the two substituted series, $r^2$=0.94 and $r^2$=0.91 for the C3 and C7 derivatives, respectively. Therefore, the reaction mechanism considered in this work satisfies the Principle of Maximum Hardness (PMH),[32] and provides an additional validation of the structures calculated for this reaction, from a Conceptual Density Functional Theory point of view.

### 3.3. Protonation effects

Of the three nitrogen atoms of triazolopyridine, N2 is experimentally described as the most favorable site for protonation[33] or for reaction with alkylating agents,[34] an observation supported by molecular orbital calculations.[35] It was interesting for us to study the effect of the protonation over the relative energies and transition barriers in the different equilibria. All the possible protonation situations in the case of the parent equilibrium were considered: the protonation of N1 or N2 in the **CLS** isomer, and all the corresponding open forms, and the protonation of the pyridinic nitrogen in **OPN1** and **OPN2** isomers. An initial observation is that the protonation of the triazolopyridine in N1 or N2 site highly stabilizes the closed form, increasing significantly the endothermic character of the open step showing transition barriers of 245 and 373 kJ mol$^{-1}$, respectively (Scheme 6).

Table 6 shows the relatives energies and proton affinities of the structures considered. The global energy minima correspond to the **CLS-N2H$^+$** isomer. The major stability and proton affinity of **CLS-N2H$^+$** respect **CLS-N1H$^+$** is coherent with the

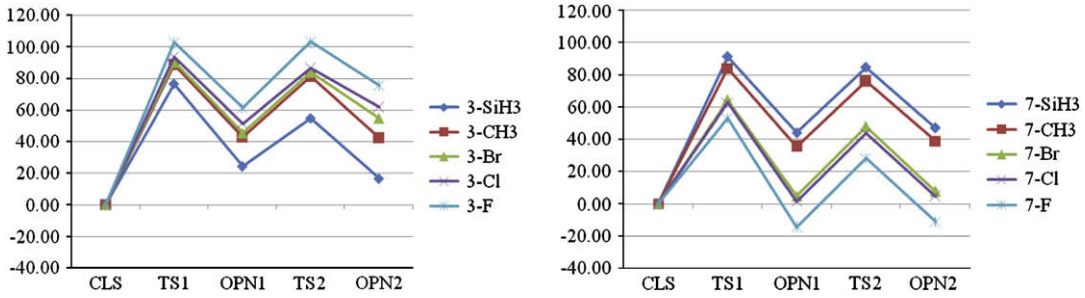


**Figure 4.** Substitution effect in the relative energies of Series 2 (kJ mol$^{-1}$).

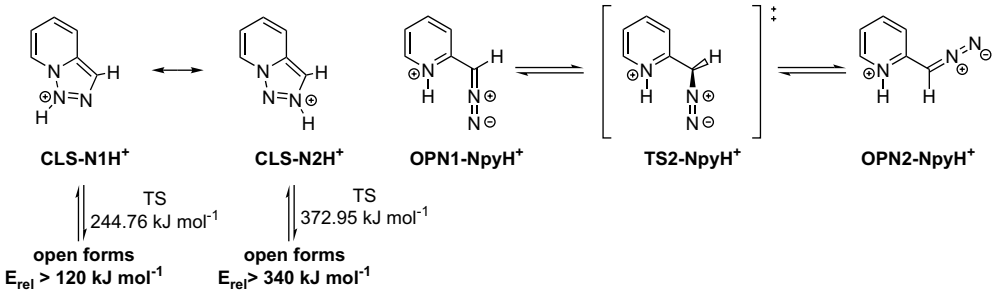


**Scheme 6.** Protonation compounds studied in this work (only the structures in a range of energy close to the absolute minima).

experimental results previously commented. The stability of the open pyridinium isomers **OPN1-NpyH**$^+$ and **OPN2-NpyH**$^+$ is lower with respect to **CLS-N2H**$^+$, albeit in a narrow energetic range (<25 kJ mol$^{-1}$).

No experimental proton affinity is available in the literature for these compounds. However, the calculated results are analogous to those of the pyridine obtained at the same computational level (PA 930.1)[36] as well as experimentally (PA 930.0).[37]

The molecular electrostatic potential (MEP) is a parameter widely used to predict chemical reactivity and tendency to form complexes. In the structures studied we have focused our attention in the MEP of the three unsubstituted triazolopyridine neutral minima (**CLS**, **OPN1**, and **OPN2**) as a descriptor of the potential interaction regions in the molecule.

Figure 6 represents the molecular electrostatic potential views of the three minima considered. **CLS** presents a big negative region in the MEP (green region) corresponding to the lone pairs of the N1 and N2 nitrogens. **OPN1** and **OPN2** show a equivalent distribution of the MEP, with the bigger negative region localized over the lone pair of the pyridinic nitrogen, and a second site close to the terminal nitrogen of the diazo system.

The values of the MEP minima are shown in Table 7. **CLS** isomer has two minima, −0.082 and −0.098, corresponding to the N1 and N2 lone pairs, respectively, where N2 is the position potentially more available to interact. This result agrees with the experimental data of protonation as it has been described before. For the open forms the clear minima corresponds to the pyridinic nitrogen lone pair (−0.087 and −0.088 in **OPN1** and **OPN2**, respectively).

**Table 6**
Relative energies of the protonated [1,2,3]triazolo[1,5-*a*]pyridine calculated at B3LYP/6-31+G** level

| Form | *E* (hartree) | Δ*E* (kJ mol$^{-1}$) | *μ* (debye) | PA (kJ mol$^{-1}$) |
|---|---|---|---|---|
| **CLS-N1H**$^+$ | −396.2307622 | 35.5 | 2.38 | 893.2 |
| **CLS-N2H**$^+$ | −396.2442786 | 0.0 | 2.33 | 924.7 |
| **OPN1-NpyH**$^+$ | −396.2366305 | 20.1 | 1.56 | 936.2 |
| **TS2-NpyH**$^+$ | −396.2200498 | 63.6 | 4.48 | 933.0 |
| **OPN2-NpyH**$^+$ | −396.2381199 | 16.2 | 3.28 | 942.9 |

**Table 7**
Minima of the molecular electrostatic potential of the studied structures

| Form | N1 | N2 | Npy |
|---|---|---|---|
| **CLS** | −0.082 | −0.098 | — |
| **OPN1** | −0.036 | — | −0.087 |
| **OPN2** | −0.030 | — | −0.088 |

### 3.4. Deprotonation effects

In tandem with the substitution effect study, we have considered analyzing the consequences of the deprotonation of the different positions of the [1,2,3]triazolo[1,5-*a*]pyridine ring over the equilibrium (Scheme 7).

Table 8 shows the energetic results of the deprotonation study. Being tautomers, it is reported the relative energy of each deprotonated structure respect the absolute minima that corresponds to the **3-DPT-CLS** form. The deprotonation produce a similar effect that the substitution by an electrodonating group (Figure 10) and the larger variations in the energetic profile occurs again in the case of the structures 3- and 7-deprotonated. The trend of the relative energies of the **3-DPT** and **7-DPT** structures is similar to the corresponding **3-SiH$_3$** and **7-SiH$_3$** derivatives but with energetic differences more pronounced.

The formation of an anion on the C3 site produces a destabilization of the closed form increasing the probability of open ones, while the opposite effect occurs when the negative charge is located on the C7 position. As we can see in Figure 7, the deprotonation of C3 make the open step clearly exothermic, while the deprotonation of C7 shows the most endothermic profile of opening reaction.

### 3.5. The special case of lithiation

The lithiation of [1,2,3]triazolo[1,5-*a*]pyridines is a regioselective process that occurs exclusively on the position C7 of the heterocyclic ring. This position in triazolopyridines does not

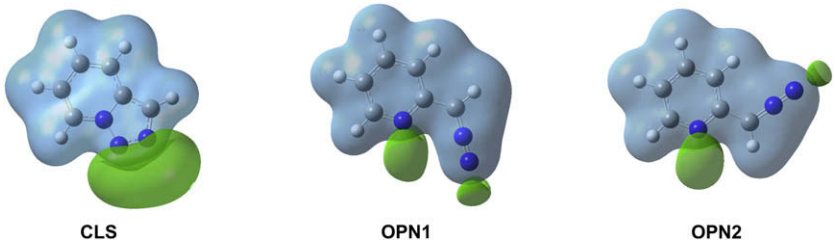


**Figure 6.** Representation of the MEP in the neutral isomers of [1,2,3]triazolo[1,5-*a*]pyridine at the +/−0.03 au isosurface. Negative regions are represented in green with positive ones in blue.

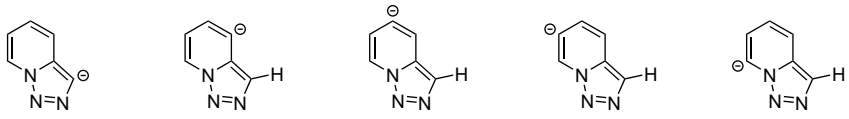


**Scheme 7.** Deprotonation compounds studied in this work.

**Table 8**
Absolute and relative energies of the deprotonated [1,2,3]triazolo[1,5-*a*]pyridine calculated at B3LYP/6-31+G** level

| Form | *E* (hartree) | Δ*E* (kJ mol$^{-1}$) | Δ*E*[a] (kJ mol$^{-1}$) | Sym | *μ* (debye) |
|---|---|---|---|---|---|
| **3-DPT-CLS** | −395.249603 | 0.0 | 91.9 | $C_s$ | 9.57 |
| **3.DPT-TS1** | −395.223438 | 68.7 | 160.6 | $C_s$ | 7.84 |
| **3-DPT-OPN1** | −395.284591 | −91.9 | *0.0* | $C_s$ | 7.07 |
| **3-DPT-TS2** | −395.269895 | −53.3 | 38.6 | $C_1$ | 8.75 |
| **3-DPT-OPN2** | −395.283704 | −89.5 | *2.3* | $C_s$ | 7.03 |
| **4-DPT-CLS** | −395.262847 | 0.0 | 57.1 | $C_s$ | 4.06 |
| **4-DPT-TS1** | −395.221094 | 109.6 | 166.7 | $C_s$ | 3.12 |
| **4-DPT-OPN1** | −395.238932 | 62.8 | 119.9 | $C_s$ | 2.15 |
| **4-DPT-TS2** | −395.223825 | 102.4 | 159.5 | $C_1$ | 3.27 |
| **4-DPT-OPN2** | −395.237291 | 67.1 | 124.2 | $C_s$ | 3.32 |
| **5-DPT-CLS** | −395.257099 | 0.0 | 72.2 | $C_s$ | 2.77 |
| **5-DPT-TS1** | −395.222509 | 90.8 | 163.0 | $C_s$ | 4.16 |
| **5-DPT-OPN1** | −395.237725 | 50.9 | 123.0 | $C_s$ | 4.97 |
| **5-DPT-TS2** | −395.226371 | 80.7 | 152.8 | $C_1$ | 5.12 |
| **5-DPT-OPN2** | −395.235614 | 56.4 | 128.6 | $C_s$ | 5.94 |
| **6-DPT-CLS** | −395.261117 | 0.0 | 61.6 | $C_s$ | 5.00 |
| **6-DPT-TS1** | −395.220903 | 105.6 | 167.2 | $C_s$ | 6.23 |
| **6-DPT-OPN1** | −395.231892 | 76.7 | 138.4 | $C_s$ | 7.98 |
| **6-DPT-TS2** | −395.223128 | 99.7 | 161.4 | $C_1$ | 7.31 |
| **6-DPT-OPN2** | −395.232364 | 75.5 | 137.1 | $C_s$ | 7.40 |
| **7-DPT-CLS** | −395.272110 | 0.0 | *32.8* | $C_s$ | 6.62 |
| **7-DPT-TS1** | −395.214044 | 152.4 | 185.2 | $C_s$ | 7.35 |
| **7-DPT-OPN1** | −395.219672 | 137.7 | 170.4 | $C_s$ | 8.24 |
| **7-DPT-TS2** | −395.209792 | 163.6 | 196.4 | $C_1$ | 7.52 |
| **7-DPT-OPN2** | −395.222872 | 129.3 | 162.0 | $C_s$ | 6.20 |

[a] Relative energies respect the global minima.

correspond to the most acidic CH. Wentrup,[38] through exchange reactions with $D_2O$, had shown that the most acidic proton is located at the position C3. It follows that the lithiation is probably led by the lone pair of the nitrogen in position '*peri*' (N1), which provides some kind of coordinating interaction with the lithium reagents.

However, as was shown previously, in the [1,2,3]triazolo[1,5-*a*]pyridine ring, N2 is usually the position most available to make interactions. Moreover, the approach of the lithium reagent in this site could orient the process to the most acidic proton in C3. In this context we have studied the thermodynamic profile of the lithiation reaction of [1,2,3]triazolo[1,5-*a*]pyridines. We have examined the lithiation in all the positions of the heterocyclic ring, but for greater understanding we focused the most significant cases, C3 and C7 lithium derivatives.

Figure 8 shows the geometries of the considered minima. As can be seen in some of the structures (**3-Li-CLS**, **3-Li-OPN2**, **7-Li-CLS**, **7-Li-OPN1**, and **7-Li-OPN2**), the lithium group is shifted with respect to the carbon. The presence of a nitrogen atom with available lone pairs in the vicinity produces the interaction with the lithium atom modifying the initial geometry. This interaction occurs with the nitrogen in alpha for **3-Li-CLS**, **7-Li-OPN1**, **7-Li-OPN2**, giving a triangular system **C-Li-N**, and with the nitrogen in beta for **3-Li-OPN2**, **7-Li-CLS** resulting in a square system **C-C-Li-N**.

The analysis of the electron density with AIM methodology allows for characterization of the systems based on their critical points. In the molecules studied, the analysis of the electron density maps (Fig. 9) has confirmed the existence of bond critical points (bcp) between the lithium and nitrogen atoms in the mentioned cases (**3-Li-CLS**, **3-Li-OPN2**, **7-Li-CLS**, **7-Li-OPN1**, and **7-Li-OPN2**).

Table 9 shows the energetic results of the two series (**3-Li** and **7-Li**) of the lithiation study. Firstly, we consider the relative energy of each series and, secondly, the relative energy with regard to the absolute minima which correspond to the **3-Li-OPN2** form.

The computed energetic profile of the two studied series of isomers is shown in Figure 10.

The isomeric equilibrium of 7-lithium derivatives follows an endothermic profile, coinciding with that described above for low electronegativity substituent groups, although in this case the stabilization of the closed isomer is increased due to the interaction Li–N (101.8 kJ mol$^{-1}$ **7-Li-TS1** vs 91.4 kJ mol$^{-1}$ **7-SiH$_3$-TS1**).

The analysis of the equilibrium of 3-lithium isomers is more significant. The profile is clearly endothermic towards the formation of **3-Li-OPN2**. Until now, in all the examples shown, there were no significant differences between the relative energies of the open isomers. The rotational step of the diazo groups was between two structures energetically equivalent. In this case, the disposition of the diazo group with respect to the ring is very relevant (Fig. 8) since it can allow or not the interaction between the lithium atom and the pyridinic nitrogen. The geometry of **3-Li-OPN2** allows the Li–N coordination, making this configuration considerably more stable (a similar effect was observed in the lithiation of aziridines).[39]

The calculated energies (Table 9) show that **7-Li-CLS** is 42.28 kJ mol$^{-1}$ more stable than **3-Li-CLS.** This result agrees with the experimental regioselectivity previously indicated. Although in both cases there is stabilization by the nitrogen lone pair, the

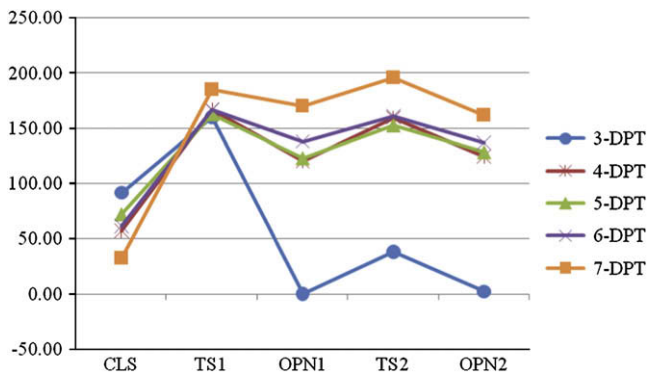


**Figure 7.** Deprotonation effect in the relative energies (kJ mol$^{-1}$) of different positions of the ring–chain interconversion reaction of [1,2,3]triazolo[1,5-*a*]pyridines calculated at B3LYP/6-31+G** level.

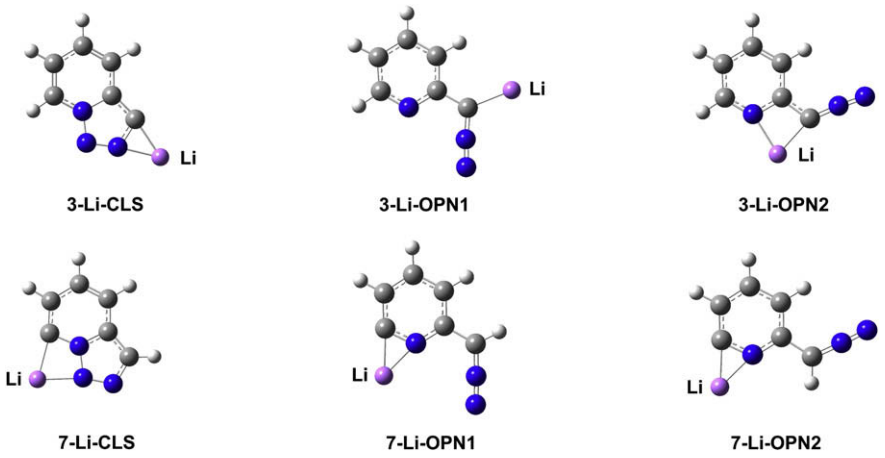


**Figure 8.** Optimized geometries of the minima in the 3- and 7-lithitium derivatives.

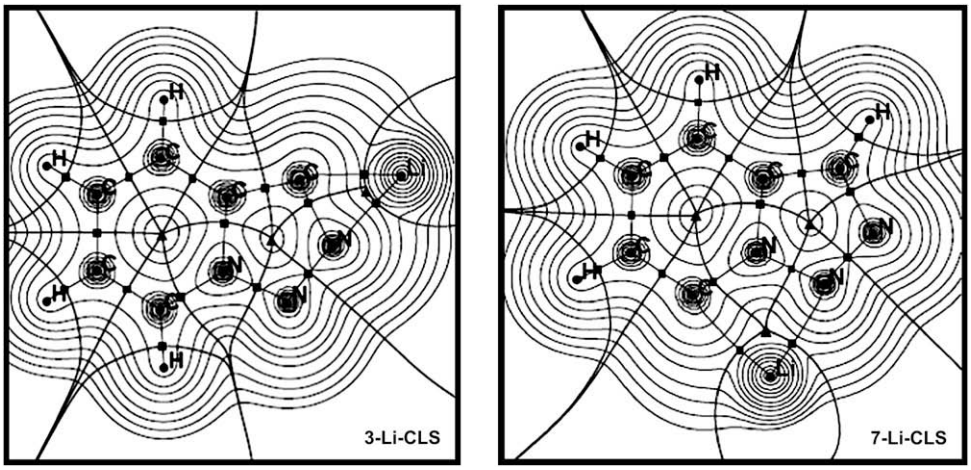


**Figure 9.** Electron density maps AIM for two representative cases.

geometry in the second case is more favorable. One possible reason is that the annular tension in the trigonal system **Li-C-N** of **3-Li-CLS** is higher than in the four-membered ring of **7-Li-CLS** (**Li-C-N-N**). Given the high availability of N2 to interact, and the major acidity of the proton in C3, the fact that the reaction experimentally goes to the C7 position could be due to a thermodynamic control based in the stability of **7-Li-CLS** with respect to **3-Li-CLS.**

**Table 9**
Absolutes and relative energies of 3- and 7-lithiated isomers calculated at the B3LYP/6-31+G** level

| Form | $E$ (hartree) | $\Delta E$ (kJ mol$^{-1}$) | $\Delta E^{a}$ (kJ mol$^{-1}$) | Sym | $\mu$ (debye) |
|---|---|---|---|---|---|
| **3-Li-CLS** | −402.799991 | 0.0 | 62.9 | $C_s$ | 2.12 |
| **3-Li-TS1** | −402.756691 | 113.7 | 176.6 | $C_s$ | 7.11 |
| **3-Li-OPN1** | −402.790139 | 25.9 | 88.8 | $C_s$ | 8.76 |
| **3-Li-TS2** | −402.779753 | 53.1 | 116.0 | $C_1$ | 7.71 |
| **3-Li-OPN2** | −402.823946 | −62.9 | *0.0* | $C_s$ | 5.56 |
| **7-Li-CLS** | −402.816094 | 0.0 | 20.6 | $C_s$ | 2.52 |
| **7-Li-TS1** | −402.770897 | 118.7 | 139.3 | $C_s$ | 1.60 |
| **7-Li-OPN1** | −402.779318 | 96.6 | 117.2 | $C_s$ | 1.57 |
| **7-Li-TS2** | −402.765976 | 131.6 | 152.2 | $C_1$ | 3.12 |
| **7-Li-OPN2** | −402.777313 | 101.8 | 122.4 | $C_s$ | 4.16 |

[a] Relative energies respect the global minima.

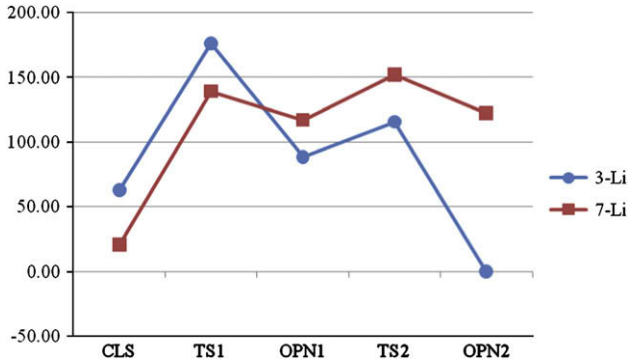


**Figure 10.** Lithiation effect in the relative energies C3 and C7 series.

## 4. Conclusion

In the present work, the ring–chain isomerism of [1,2,3]triazolo[1,5-*a*]pyridines has been theoretically studied and discussed. The results shows the important effect of the substitution over the equilibrium, specially in the C3 and C7 sites of the triazolopyridine ring, in function of the electronic properties of the functional

groups. Therefore, we examined the deprotonation, which produced an effect qualitatively similar to the substitution by electron releasing groups. The position of the protonation and the effect of protonation and deprotonation over the isomeric equilibrium have been discussed and some results are coherent with the experimental data described in the literature. Finally, a specific study of the regioselective reaction of lithiation has been realized deducing of our result that the process could be explained by a thermodynamic criterion due to the relative stability of the lithio-derivatives.

## Acknowledgements

This work was carried out with financial support from the Ministerio de Educación y Ciencia (Project No. CTQ2007-61901/BQU and CTQ2006-15672-C05-03) and Comunidad Autónoma de Madrid (Project MADRISOLAR, ref. S-0505/PPQ/0225). Thanks are given to the CTI (CSIC) and CESGA for allocation of computer time.

## References and notes

1. Plas, H. C. v. d *Ring Transformation of Heterocycles*; Academic: London, 1973.
2. Valters, R. E.; Fleitsch, W. *Ring–Chain Tautomerism*; Plenum: New York, NY, 1985.
3. Zelenin, K. N.; Alekseev, V. V. *Khim. Geterotsikl. Soedin.* **1988**, 3–19.
4. Zelenin, K. N.; Alekseev, V. V. *Khim. Geterotsikl. Soedin.* **1992**, 851–860.
5. Wamhoff, H. Comprehensive Heterocyclic Chemistry; Elsevier: Oxford, 1984; Vol. 5, pp 686–691.
6. Fan, W. Q.; Katritzky, A. R. *Comprehensive Heterocyclic Chemistry II*; Elsevier: Oxford, 1996; Vol. 4, 1–126.
7. Trifonov, R. E.; Alkorta, I.; Ostrovskii, V. A.; Elguero, J. *Heterocycles* **2000**, *52*, 291–302.
8. Jones, G.; Sliskovic, D. R.; Foster, B.; Rogers, J.; Smith, A. K.; Wong, M. Y.; Yarham, A. C. *J. Chem. Soc., Perkin Trans. 1* **1981**, 78–81.
9. Abarca, B.; Ballesteros, R.; Rodrigo, G.; Jones, G.; Veciana, J.; Vidal-Gancedo, J. *Tetrahedron* **1998**, *54*, 9785–9790.
10. Abarca, B.; Alkorta, L.; Ballesteros, R.; Blanco, F.; Chadlaoui, M.; Elguero, J.; Mojarrad, F. *Org. Biomol. Chem.* **2005**, *3*, 3905–3910.
11. Becke, A. D. *J. Chem. Phys.* **1993**, *98*, 5648–5652.
12. Lee, C. T.; Yang, W. T.; Parr, R. G. *Phys. Rev. B* **1988**, *37*, 785–789.
13. Hariharan, P. C.; Pople, J. A. *Theor. Chim. Acta* **1973**, *28*, 213–222.
14. Frisch, M. J.; Trucks, G. W.; Schlegel, H. B.; Scuseria, G. E.; Robb, M. A.; Cheeseman, J. R.; Montgomery, J. J. A.; Vreven, T.; Kudin, K. N.; Burant, J. C.; Millam, J. M.; Iyengar, S. S.; Tomasi, J.; Barone, V.; Mennucci, B.; Cossi, M.; Scalmani, G.; Rega, N.; Petersson, G. A.; Nakatsuji, H.; Hada, M.; Ehara, M.; Toyota, K.; Fukuda, R.; Hasegawa, J.; Ishida, M.; Nakajima, T.; Honda, Y.; Kitao, O.; Nakai, H.; Klene, M.; Li, X.; Knox, J. E.; Hratchian, H. P.; Cross, J. B.; Bakken, V.; Adamo, C.; Jaramillo, J.; Gomperts, R.; Stratmann, R. E.; Yazyev, O.; Austin, A. J.; Cammi, R.; Pomelli, C.; Ochterski, J. W.; Ayala, P. Y.; Morokuma, K.; Voth, G. A.; Salvador, P.; Dannenberg, J. J.; Zakrzewski, V. G.; Dapprich, S.; Daniels, A. D.; Strain, M. C.; Farkas, O.; Malick, D. K.; Rabuck, A. D.; Raghavachari, K.; Foresman, J. B.; Ortiz, J. V.; Cui, Q.; Baboul, A. G.; Clifford, S.; Cioslowski, J.; Stefanov, B. B.; Liu, G.; Liashenko, A.; Piskorz, P.; Komaromi, I.; Martin, R. L.; Fox, D. J.; Keith, T.; Al-Laham, M. A.; Peng, C. Y.; Nanayakkara, A.; Challacombe, M.; Gill, P. M. W.; Johnson, B.; Chen, W.; Wong, M. W.; Gonzalez, C.; Pople, J. A. *Gaussian-03*; Gaussian: Wallingford, CT, 2003.
15. Bader, R. F. W. *Atoms in Molecules: A Quantum Theory*; Clarendon: Oxford, 1990.
16. Biegler-König, F.W.; Bader, R. F. W.; Tang, T. H. *J. Comput. Chem.* **1982**, *3*, 317.
17. Popelier, P. L. A.; Bone, R. G. A. MORPHY98, a topological analysis program, UMIST: England, Europe, 1999.
18. Reed, A. E.; Curtiss, L. A.; Weinhold, F. *Chem. Rev.* **1988**, *88*, 899–926.
19. Glendening, E. D.; Reed, A. E.; Carpenter, J. E.; Weinhold, F. NBO program: NBO 3.1 Program.
20. Alkorta, I.; Villar, H. O.; Arteca, G. A. *J. Comput. Chem.* **1993**, *14*, 530–540.
21. Alkorta, I.; Bachs, M.; Perez, J. J. *Chem. Phys. Lett.* **1994**, *224*, 160–165.
22. Solimannejad, M.; Alkorta, I.; Elguero, J. *J. Phys. Chem. A* **2007**, *111*, 2077–2083.
23. Becke, A. D.; Edgecombe, K. E. *J. Chem. Phys.* **1990**, *92*, 5397–5403.
24. Silvi, B.; Savin, A. *Nature* **1994**, *371*, 683–686.
25. Guner, V.; Khuong, K. S.; Leach, A. G.; Lee, P. S.; Bartberger, M. D.; Houk, K. N. *J. Phys. Chem. A* **2003**, *107*, 11445–11459.
26. Restrepo-Cossio, A. A.; Gonzalez, C. A.; Mari, F. *J. Phys. Chem. A* **1998**, *102*, 6993–7000.
27. Davis, B. R.; Ibers, J. A. *Inorg. Chem.* **1970**, *9*, 2768–2774.
28. Tredgold, R. H.; Allen, R. A.; Hodge, P. *Thin Solid Films* **1987**, *155*, 343–352.
29. Hammond, G. S. *J. Am. Chem. Soc.* **1955**, *77*, 334–338.
30. Parr, R. G.; Pearson, R. G. *J. Am. Chem. Soc.* **1983**, *105*, 7512–7516.
31. Geerlings, P.; De Proft, F.; Langenaeker, W. *Chem. Rev.* **2003**, *103*, 1793–1874.
32. Pearson, R. G. *Chemical Hardness: Applications from Molecules to Solids*; Wiley-VCH GMBH: Weinheim, 1997.
33. Armarego, W. L. *J. Chem. Soc.* **1965**, 2778–2787.
34. Abarca, B.; Ballesteros, R.; Mojarrad, F.; Metni, M. R.; Garcia-Granda, S.; Perez-Carreño, E.; Jones, G. *Tetrahedron* **1991**, *47*, 5277–5286.
35. Jones, G.; Richardson, C. M.; Yates, P. C.; Hajós, G.; Timari, G. *Tetrahedron* **1993**, 4307–4314.
36. Blanco, F.; O'Donovan, D. H.; Alkorta, I.; Elguero, J. *Struct. Chem.* **2008**, *19*, 339–352.
37. NIST-Chemistry-Webbook.http://webbook.nist.gov/chemistry/ (accessed June 2005).
38. Wentrup, C. *Helv. Chim. Acta* **1978**, *61*, 1755–1764.
39. Capriati, V.; Florio, S.; Luisi, R.; Musio, B.; Alkorta, I.; Blanco, F.; Elguero, J. J. *Struct. Chem.* **2008**, *19*, 785–792.